COBEM 2023 27TH INTERNATIONAL CONGRESS OF MECHANICAL ENGINEERING

ABCM Brazilian Society of Mechanical Sciences and Engineering
27th ABCM International Congress of Mechanical Engineering
December 04-08, 2023, Florianópolis-SC, Brazil

COB-2023-0365
EXPERIMENTAL ANALYSIS OF THE INTERACTIONS BETWEEN AIR MICROBUBBLES AND OIL DROPLETS IMMERSED IN WATER INSIDE A MODEL FLOTATOR

Tiago Henrique Leitão Dalcuche
Pedro Ignacio da Silva Morales
Thiago Sirino
Henrique Stel de Azevedo
Moisés Alves Marcelino Neto
Rigoberto Eleazar Melgarejo Morales
Multiphase Flow Research Center – NUEM, Graduate Program in Mechanical and Materials Engineering – PPGEM, Federal University of Technology of Parana, Brazil
tdalcuche@alunos.utfpr.edu.br
pmorales@alunos.utfpr.edu.br
thiagosirino@hotmail.com
stel.henrique@gmail.com
mneto@utfpr.edu.br
rmorales@utfpr.edu.br

Abstract: ***Upon extraction from the well, the crude oil, gas and water are subjected to a phase separation process, usually by using a sequence of separator vessels. This process involves separating the gas phase, the oil-rich phase and the water-rich phase. This latter, consisting of water and dispersed oil and gas, is then directed to a flotation system, which makes use of several separation techniques such as gravity separation and flotation to separate the oil and water phases. The interactions between air microbubbles and oil droplets in water are of great importance in flotation. In this study, the behavior of air microbubbles and oil droplets in a model flotator was experimentally investigated. The experiments were conducted by injecting microbubbles and oil droplets into a water-filled model flotator under a continuous inflow of water at a constant flowrate of 25 l/h. The experimental apparatus is under atmospheric pressure. The main focus was to evaluate the process of adhesion of microbubbles and droplets and to determine the influence of the continuous phase on the dispersed phases. To achieve this, a high-speed camera was used to capture the behavior of the microbubbles and droplets in real-time. Our experimental results showed that the adhesion between microbubbles and droplets is highly contingent upon the velocity and the diameter ratios. Specifically, adhesion is more likely to occur when the velocity ratio approaches unity. Analysis of the contact angle further indicates that, within our experimental conditions, the region behind the droplet, known as the wake, exhibits favorable conditions for adhesion. A comparative examination of the bubble velocity angle and the droplet velocity angle indicates that the movement of both bubbles and droplets is governed by the flow of the continuous phase. Overall, the experimental analysis herein discussed provides valuable insights into the behavior of air microbubbles and oil droplets in water and their interactions under different conditions. The findings in the present work can be useful in designing and optimizing flotation systems for oil-water separation in the industry.***

Keywords: *Flotation, Phase separation , Microbubbles, Oil droplets, Adhesion.*

1. INTRODUCTION

Oil well production is inherently multiphase, consisting predominantly of water, oil, and gas (Thomas, 2001). Therefore, it is necessary to separate the phases that have commercial value from those that have not. The phase separation process involves several stages and pieces of equipment (Stewart & Arnold, 2008). The produced water, although lacking commercial value, must be treated to comply with current environmental regulations. Brazilian environmental law stipulates that water must not contain more than 39 mg/l of fatty oils (Resolution Nº 393, August 8, 2007). One of the ending pieces of equipment responsible for water treatment in the processing chain is the flotation unit.

The flotation process involves injecting microbubbles into a continuous fluid to assist in the removal of an undesired dispersed phase (Edzwald, 1995; Moosai & Dawe, 2003; Peleka & Matis, 2016). Although not originally designed for this purpose, flotation can be used in the oil and gas industry. There are indications that this technology was firstly used in produced water treatment in the early 21st century (Piccioli et al., 2020). As a result, there are still several unexplored gaps in this field of knowledge.

One such research opportunity lies in the interactions between droplets and dispersed bubbles in water. This is because flotation is generally used in cases where the impurity is a solid, whereas in this work the impurity is essentially a fluid, which significantly alters the phenomenon. Interaction can occur in several ways, the main one being the encapsulation process in the droplet-bubble case. For the encapsulation to occur, a droplet and a bubble must come into contact. Subsequently, the water film between them drains, and the droplet encapsulates the bubble, forming a compound droplet (Nguyen & Schulze, 2004).

The objective of this work is to analyze and understand the interactions between droplets, bubbles and the continuous phase and the dynamics of the adhesion process.

2. METHODOLOGY AND EXPERIMENTAL SETUP

The developed flotation model employed in this study, as illustrated in Figure 1, incorporates two distinct inlets: an upper inlet designed for the injection of water (25 L/h) and droplets (0.06 L/h), and a lower inlet for the introduction of water (30 L/h) and bubbles (4% volume fraction). We utilized USP mineral oil with a density of 832.28 ± 2.14 kg/m³ and a viscosity of 30.45 cP. Oil breaking was achieved through the controlled adjustment of a partially closed needle valve. The bubbles were comprised of atmospheric air and were generated by saturating and subsequently depressurizing the mixture near the entrance, utilizing an orifice plate with a diameter of 0.8 mm. Both water flow lines were precisely measured using Coriolis flow meters, while the oil flow was regulated by a syringe pump. The gas flow rate was not directly measured but was estimated as the difference between the dissolved volume in the tank and the dissolved volume under atmospheric conditions. Since an exact value was not crucial for comprehending the dynamics of individual interactions between droplets and bubbles, an approximation sufficed. The equipment boasts dimensions of 300 mm in length, 180 mm in height, and 20 mm in thickness. Immediately following the inlet, the flow encounters a 90-mm baffle positioned 60 mm from the inlet. This baffle induces moderate mixing in the inlet region, thereby enhancing the likelihood of collisions between bubbles and droplets. On the upper face of the flotation system, two openings are present. The first is the Gas Inlet, enabling the injection of gas to increase the pressure inside the chamber, while the other serves as the gas relief, where pressure is regulated using a pressure control valve.

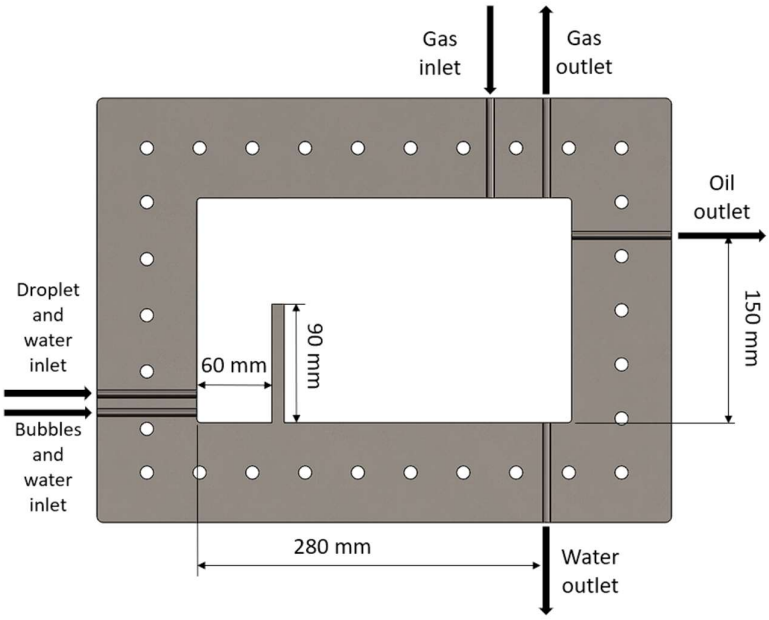

Figure 1 – Model flotation system

A high-speed camera is positioned orthogonally – as shown in Figure 2 – to capture footage in three locations, called *windows*. Each of these windows has dimensions of 17.4 cm x 17.4 cm, equally spaced along the direction of the inlet in the region preceding the baffle. The upper part of the windows is positioned at a distance of 80 mm from the flotator base. This region was chosen so it would not be so close to the inlet – where intense turbulence occurs – and not so distant from the inlet either – where most of the compound droplets have already formed. The oil phase was dyed with a red colorant so bubbles and droplets could be easily distinguished from each other.

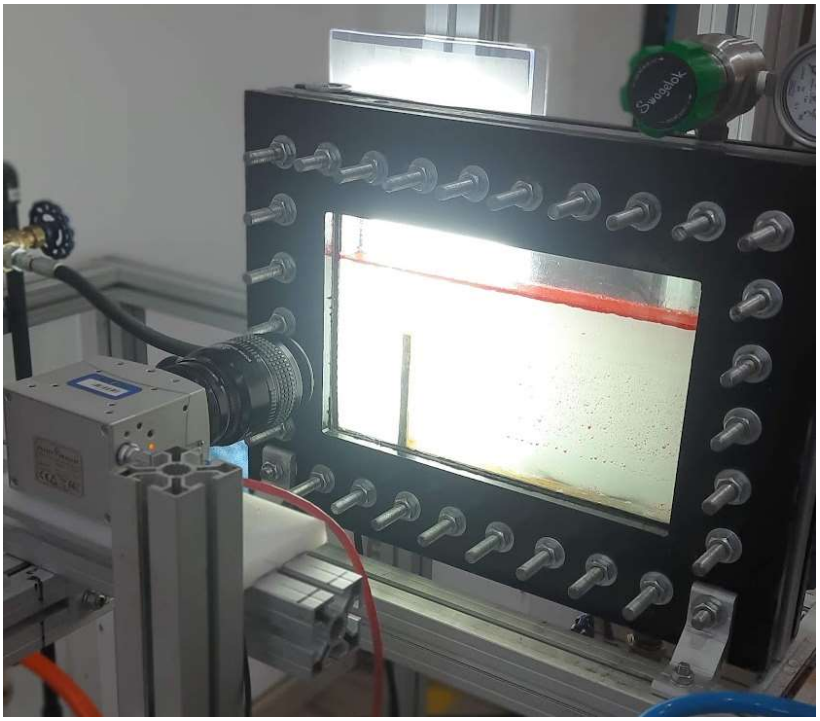

Figure 2 – Experimental Apparatus .

For each of the three windows (J1, J2 and J3) as shown in Figure 3, three sets of videos were recorded. Therefore, a total of 9 sets of videos were obtained. Each film has a duration of seven and a half seconds, due to the camera storage limit. A frame rate of 200 frames per second was utilized, resulting in a total of 1470 frames per battery set. In each of the 13230 frames, a meticulous search to identify droplets and bubbles undergoing the process of adhesion was carried out.

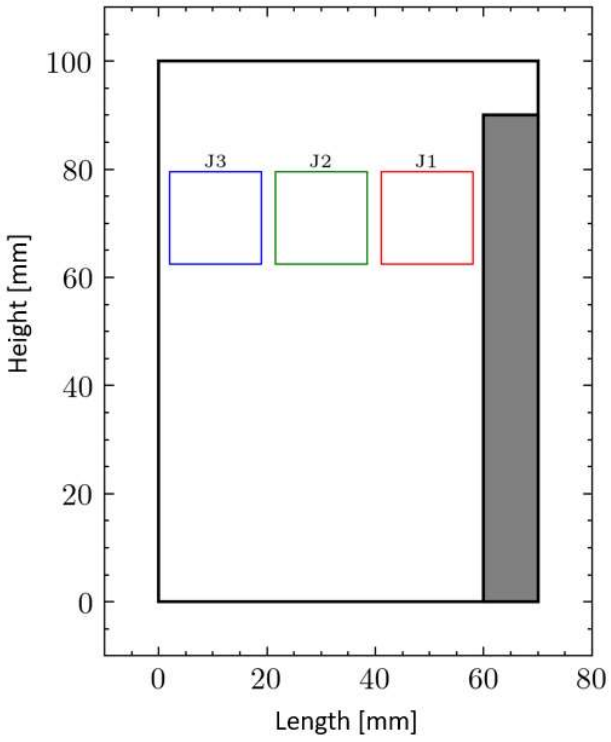

Figure 3 – Example of a cropped region of interest

When the formation of a compound droplet was observed, the region of interest was cropped and tagged, as seen in Figure 4. For illustration purposes, only every 5th frame is shown in the figure. The bubbles can be distinguished by a dark edge and a body clear. The droplets are dyed red and have a darker body with less contrast on the edge.

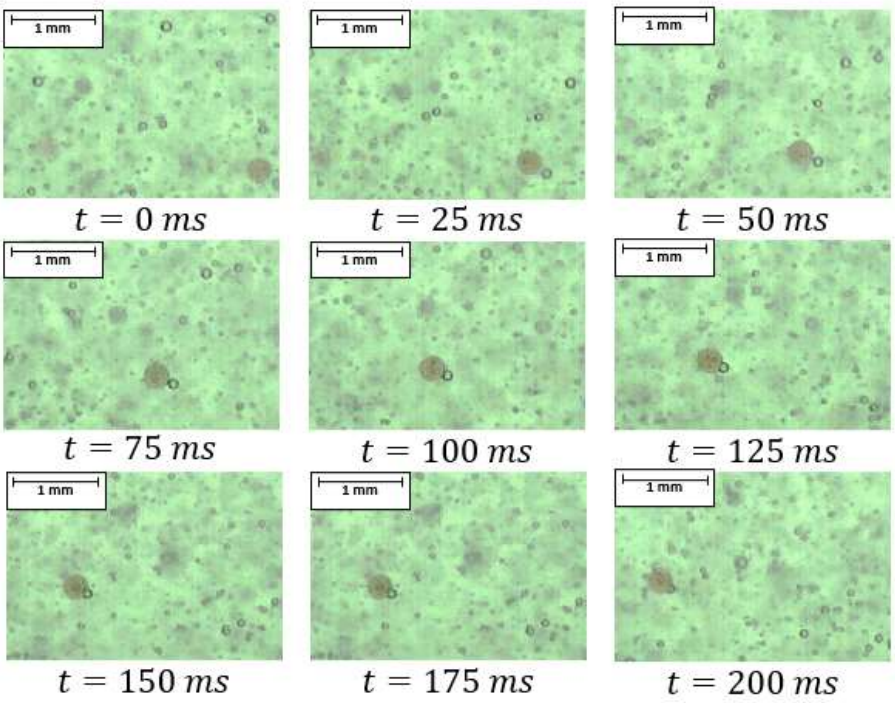

Figure 4 – Example of a cropped region of interest

The analysis of particle position and diameter was carried out with the aid of a specialized Python program designed and written specifically for this purpose. This program uses the Hough Circle Transform (HCT), available through the OpenCV library, to predict the radius and position of the bubbles or droplets. Since HCT relies heavily on the quality each image and this quality varies even within the same set of images, it is not possible to predict its accuracy. Therefore, the program is designed to operate in a semi-automatic manner. In cases where the program provided a reliable prediction, the measurement was accepted. Otherwise, if the program's output was deemed inaccurate and manual measurement were performed as an alternative approach to ensure precision and accuracy. This combination of automated and manual measurements ensured a robust and reliable assessment of particle properties within the captured images.

2.1 Determining when adhesion occurs

The induction time, that is, the period during which the thin liquid film of the continuous phase forms and breaks, can be estimated by analyzing the temporal evolution of the distance between the droplet surface and the bubble surface. According to Derjaguin and Dukhin (1961), the continuous liquid film between the droplet and the bubble begins to drain when it reaches a thickness of 100 nm. Considering the spatial resolution of the filmed images as 10.16 μm/pixel, the liquid film would have a length of approximately 0.01 pixels, rendering it visually undetectable.

Given this microscopic nature of the film, an approximation is made. Through the study of positions, it is observed that in the initial moments an approach occurs, referred to as the "Before" period. This is followed by a near-zero stagnation, known as the "During" period. Subsequently, the film thickness value abruptly reaches a negative value, initiating the "After" period. This methodology is illustrated in in Figure 5. The period before the encounter is represented in yellow, and the time steps during which the bubble and the droplet are in contact are shown in blue. Finally, the period after the sudden reduction in thickness to negative values, represented in green, is considered as the post-drainage period, that is, the moment when the droplet begins to spread around the bubble, encapsulating it.

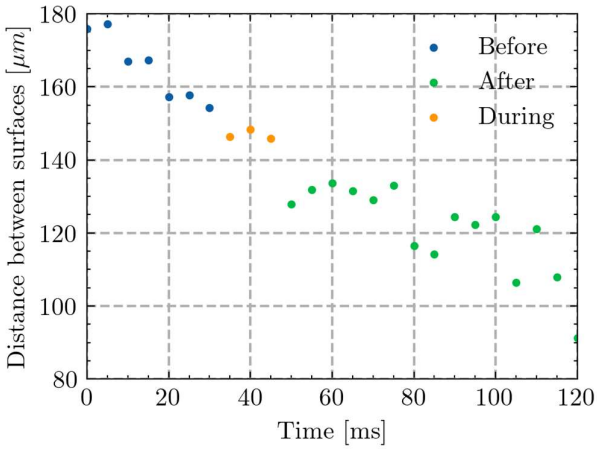

Figure 5 – Distance between bubble and droplet over time

2.2 Contact and Velocity Angle

The contact angle plays a crucial role in the adhesion process as it governs the time during which a bubble remains in contact with the droplet surface, facilitating the phenomenon of flotation (Albijanic et al., 2010). In Figure 6 the reference angle (0°) corresponds to the direction of the droplet's velocity vector. Theoretically, the optimal contact angle is 180° since it allows the maximum possible duration time during which drainage can take place, if both bubble and droplet are flowing in the same direction. The contact angle is measured at the timesteps where the methodology previously presented in chapter 2.1 indicates "During" adhesion.

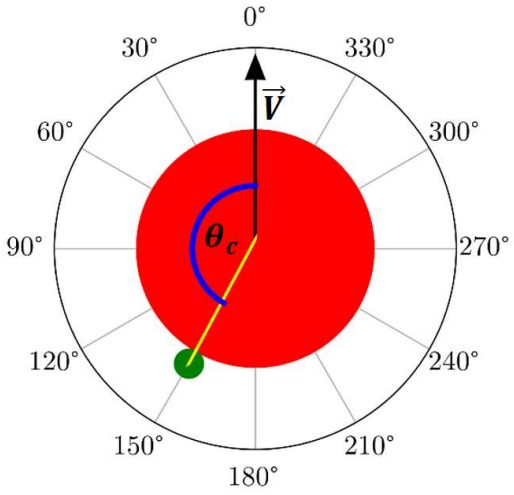

Figure 6 – Contact angle from the perspective of the droplet

The angle θ_c – shown in Figure 6 – is measured for each of the identified compound droplets, and it represents the angle between the velocity vector of the droplet ($\overrightarrow{V_d}$) and the intercenter vector ($\overrightarrow{r_{itc}}$). This angle can be mathematically described as follows:

$$\cos(\theta_c) = \frac{\langle \overrightarrow{V_d}, \overrightarrow{r_{itc}} \rangle}{|\overrightarrow{V_d}| . |\overrightarrow{r_{itc}}|}, \tag{1}$$

isolating θ_c, comes:

$$\theta_c = \cos^{-1}\left[\frac{V_{x_d}(x_b - x_d) + V_{y_d}(y_b - y_d)}{\sqrt{V_{x_d}^2 + V_{y_d}^2} . \sqrt{(x_b - x_d)^2 + (y_b - y_d)^2}}\right], \tag{2}$$

where x and y represent the position coordinates and the subscripts b and d represent the bubble and the droplet, respectively. The same process can be performed with the bubble velocity as the referential angle.

3. RESULTS

The present section presents the outcomes and analyses derived from observing the formation of 77 compound droplets. The results obtained shed light on several aspects of the droplet formation process, providing valuable information for further understanding and investigation. Additionally, the data collected during the study serve as a foundation for the subsequent discussions and conclusions presented in this article.

The observation of the 77 compound droplets during their formation allowed a comprehensive examination of their properties. Notably, particular attention was given to the contact angles exhibited by these droplets, as they serve as key indicators of interfacial phenomena.

These findings add to the existing knowledge on compound droplet formation and provide valuable insights into the underlying mechanisms at play. The subsequent sections delve deeper into the implications of these results and discuss their implications in the context of relevant theoretical frameworks and previous research.

3.1 Pre-Collision Velocity Ratio

In each case, the pre-collision velocity was measured through linear regression. Given the inherent errors in semi-manual position measurements, positions of both the droplet and the bubble were recorded as functions. Regressions were performed for both the droplet and the bubble in the X and Y axes, followed by the determination of the resulting velocity through the formula:

$$V = \sqrt{V_x^2 + V_y^2}. \tag{3}$$

This variable governs the dynamics of the collision between the droplet and the bubble. The statistical distribution of the velocity ratios was evaluated for each formed compound droplet, as shown in Figure 7.

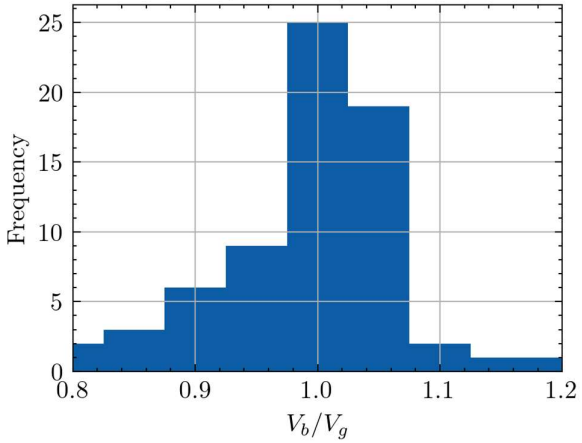

Figure 7 – Velocity ratios histogram

As anticipated, pre-collision velocity ratios that enable agglomerate formation tend to be close to unity. In other words, for the flotation process to occur, the velocities of the droplet and of the bubble must be of comparable magnitudes.

3.2 Adhesion contact angle

The results show measures by taking both the direction of the bubble's velocity vector as 0° (θ_{cb}) and the droplet velocity as the reference point (θ_{cd}). For each and every compound droplet formation process observed, the contact angles of every timestep during adhesion were measured. For each compound droplet, the initial contact angle (θ_{ci}), the final contact angle (θ_{cf}) and the average contact angle ($\overline{\theta_c}$) were measured. All three of these angles were measured for both the bubble velocity referential and the droplet velocity referential. The histogram of the average contact was plotted, as seen in Figure 8. In order to facilitate the interpretation of the graph and present a normal distribution in both graphs, the bubble reference graphs range from -180° to +180° (a), while the drop reference graphs range from 0° to 360° (b).

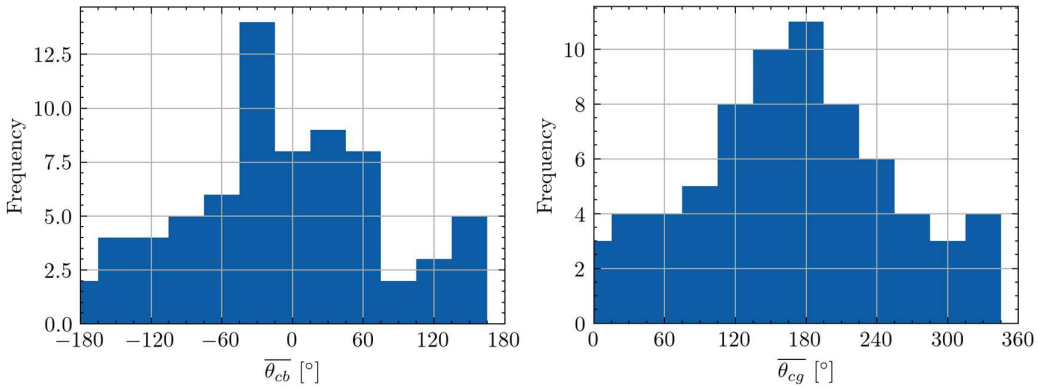

a) b)

Figure 8 – Average contact angle during adhesion

Both histograms complementarily present similar results. It can be stated that flotation occurs preferably when the bubble is located at the wake of the drop and when the drop is on a collision path with the bubble. Although these two conclusions may seem intuitive their validation is not trivial, highlighting the worth of the methodology developed in this study. The histograms of the initial and the final contact angles do not provide a different perspective from the one presented in the average angle. However, a variable can still be derived: the variation of the contact angle during adhesion ($\Delta\theta_c$). The statistical distributions were also evaluated in the form of histograms, shown in Figure 9, the first one using the bubble velocity as reference (a) and the second using the droplet velocity (b). Positive values indicate rotation in the counterclockwise direction and the negative values represent clockwise movement.

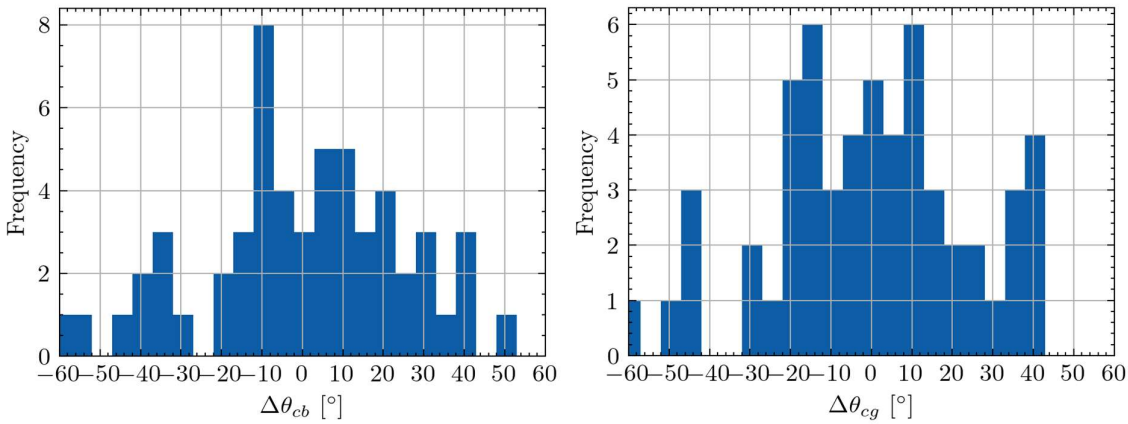

a) b)

Figure 9 – Variation of the contact angle during adhesion

These statistical distributions demonstrate that, overall, there is a small deviation between the initial and the final contact angles. It is also observed that values close to 90 degrees are of difficult observation, thereby reinforcing the theory of slippage, which posits that when the bubble and the droplet are side by side, contact ceases to occur (Nguyen & Schulze, 2004).

3.3 Diameter ratio

Another noteworthy variable for analysis is the diameter ratio. It is worth noting, as depicted in Figure 10, that diameter ratios ranging from 0.2 to 0.25 exhibit a higher occurrence rate. Furthermore, the largest observed diameter ratio is 0.4265, suggesting a maximum value of the diameter ratio for which flotation can occur.

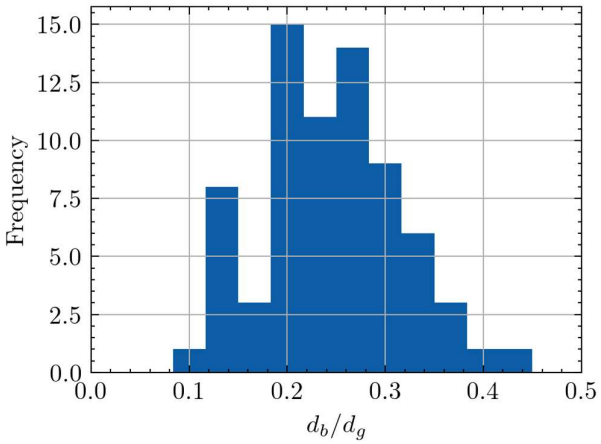

Figure 10 – Diameter ratio statistical distribution

In order to gain a broader understanding of this diameter relationship, a graph plotting the bubble diameter on the x-axis against the droplet diameter on the y-axis is constructed, as shown in Figure 11. In this case we can observe that there is a monotonic relationship between bubble diameter and droplet diameter. This means that when one grows the other does grow too. It can be also noted that there is a higher occurrence of diameter ratios near 0.25, indicating an optimum relationship.

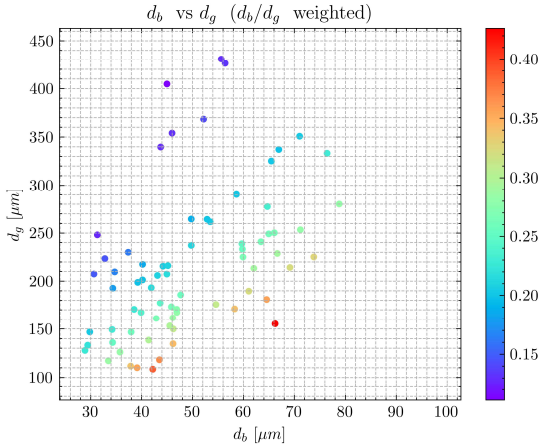

Figure 11 – Bubble diameter versus droplet diameter

4. CONCLUSIONS

The results presented in this study provide valuable insights into the formation and behavior of compound droplets. Through careful observation of 77 compound droplets, several key variables were analyzed, including the pre-collision velocity ratio, adhesion contact angle and diameter ratio.

Regarding the pre-collision velocity ratio, it was observed that agglomerate formation tends to occur when the velocities of the droplet and of the bubble are of comparable magnitudes. This finding highlights the importance of matching velocities for the flotation process to take place effectively.

Analyses of the adhesion contact angle revealed important trends. The average contact angle was found to be a reliable indicator, showing that flotation is more likely to occur when the bubble is located at the wake of the drop and when the drop is on a collision path with the bubble.

The analysis of the diameter ratio demonstrated that diameter ratios in the range of 0.2 to 0.25 exhibit a higher occurrence rate, with a maximum observed value of 0.4265. This implies that there exists an optimum ratio for which flotation can occur most favorably. The monotonic relationship observed between bubble diameter and droplet diameter further emphasizes the interdependence of these variables.

These findings contribute to the existing knowledge on compound droplet formation and provide valuable insights into the underlying mechanisms governing their behavior. The observed trends in the pre-collision velocity ratio, adhesion contact angle and diameter ratio offer practical implications for designing and optimizing flotation processes involving compound droplets.

It is important to observe that further research is warranted to deepen our understanding of the complex interfacial dynamics involved in compound droplet systems. Investigating the mechanisms behind the observed trends and conducting experiments with multiple fluid systems will provide a broader understanding of the factors influencing the formation and behavior of compound droplets.

5. ACKNOWLEDGEMENTS

"This study was financed by the Human Resource Program of The Brazilian National Agency for Petroleum, Natural Gas, and Biofuels – PRH-ANP – FINEP Management, contractual instrument n° 0.1.19.0240.00, Ref 0431/19 - PRH21-UTFPR".

6. REFERENCES

Albijanic, B., Ozdemir, O., Nguyen, A. V., & Bradshaw, D. (2010). A review of induction and attachment times of wetting thin films between air bubbles and particles and its relevance in the separation of particles by flotation. *Advances in Colloid and Interface Science*, *159*(1), 1–21. https://doi.org/10.1016/j.cis.2010.04.003

Resolução nº 393, 8 de agosto de 2007, Ministério do Meio Ambiente 72 (2007).

Derjaguin, B. V., & Dukhin, S. S. (1961). Theory of flotation of small and medium-size particles. *Institution of Mining and Metallurgy*, *43*(1–4), 241–266. https://doi.org/10.1016/0079-6816(93)90034-S

Edzwald, J. K. (1995). Principles and applications of dissolved air flotation. *Water Science and Technology*, *31*(3–4), 1–23. https://doi.org/10.1016/0273-1223(95)00200-7

Moosai, R., & Dawe, R. A. (2003). Gas attachment of oil droplets for gas flotation for oily wastewater cleanup. *Separation and Purification Technology*, *33*(3), 303–314. https://doi.org/10.1016/S1383-5866(03)00091-1

Nguyen, A. V., & Schulze, H. J. (2004). *Colloidal science of flotation*. CRC Press.

Peleka, E. N., & Matis, K. A. (2016). Hydrodynamic aspects of flotation separation. *Open Chemistry*, *14*(1), 132–139. https://doi.org/10.1515/chem-2016-0014

Piccioli, M., Aanesen, S. V., Zhao, H., Dudek, M., & Øye, G. (2020). Gas Flotation of Petroleum Produced Water: A Review on Status, Fundamental Aspects, and Perspectives. *Energy and Fuels*. https://doi.org/10.1021/acs.energyfuels.0c03262

Stewart, M., & Arnold, K. (2008). *Gas - Liquid and Liquid-Liquid Separator*.

Thomas, J. E. (2001). *Fundamentos da engenharia de petróleo* (1st ed.). Editora Interciência Ltda.

7. RESPONSIBILITY NOTICE

The authors are the only responsible for the printed material included in this paper.